

Timing characterization of MALTA and MALTA2 pixel detectors using Micro X-ray source

G. Dash¹ P. Allport² I. Asensi Tortajada³ P. Behera¹ D.V. Berlea⁴ D. Bortoletto⁵ C. Buttar⁶ V. Dao³ L. Fasselt⁴ L. Flores Sanz de Acedo³ M. Gazi⁵ L. Gonella⁷ V. Gonzalez⁸ G. Gustavino³ S. Haberl³ T. Inada³ P. Jana¹ L. Li² H. Pernegger³ P. Riedler³ W. Snoeys³ C.A Solans Sanchez³ M. van Rijnbach³ M. Vazquez Nunez^{3,8} A. Vijay¹ J. Weick³ S. Worm⁴

¹*Indian Institute of Technology Madras, Chennai, India*

²*University of Birmingham, Birmingham, United Kingdom*

³*CERN, Geneva, Switzerland*

⁴*DESY, Zeuthen, Germany*

⁵*University of Oxford, Oxford, UK*

⁶*University of Glasgow, Glasgow, United Kingdom*

⁷*Università degli Studi di Trieste, Trieste, Italy*

⁸*Universitat de València, València, Spain*

E-mail: ganapati.dash@cern.ch

ABSTRACT: The MALTA monolithic active pixel detector is developed to address the challenges anticipated in future high-energy physics detectors. As part of its characterization, we conducted fast-timing studies necessary to provide a figure of merit for this family of monolithic pixel detectors. MALTA has a metal layer in front-end electronics, and the conventional laser technique is not suitable for fast timing studies due to the reflection of the laser from the metallic surface. X-rays have been employed as a more effective alternative for penetration through these layers. The triggered X-ray set-up is designed to study timing measurements of monolithic detectors. The timing response of the X-ray set-up is characterized using an LGAD. The timing response of the MALTA and MALTA2 pixel detectors is studied, and the best response time of MALTA2 pixel detectors is measured at about 2 ns.

KEYWORDS: Particle tracking detectors (Solid-state detectors); Radiation-hard detectors; Solid state detectors

Contents

1	Introduction	1
2	MALTA and MALTA2 Pixel detectors	2
3	Micro-X-ray set-up at CERN	2
3.1	Micro-X-ray source	3
3.2	Geant4 Simulation for X-ray tube	4
4	Test set-up with LGAD	5
5	Results from LGAD	5
5.1	Characterization of Micro X-ray tube	6
5.2	Timing performance of LGAD	6
6	Measurements with MALTA and MALTA2	8
6.1	Measurements using MALTA sample	8
6.2	Measurements using MALTA2 sample	8
7	Results	10
8	Conclusion	12

1 Introduction

Pixel detectors are crucial in particle physics experiments due to their ability to precisely capture and record the individual locations of particle interactions[1]. Their high spatial resolution and fine granularity contribute to improved tracking, help in analyzing complex event topologies, and enhance the overall performance of experiments in unraveling fundamental aspects of particle behavior and interactions. The increasing energy and luminosity of the Large Hadron Collider in CERN[2][3] requires radiation hard pixel detectors[4] to sustain the environment. Therefore, there is a constant effort to make efficient and thinner pixel detectors that would be suitable for high luminosity collisions in terms of radiation hardness, high detection efficiency with low noise, dead time, and delay time. Monolithic silicon pixel detectors [5][6] are found to have better precision, better radiation hardness, and lower noise than traditional bump-based detectors with large area production, lower cost, and lower material usage. Such an attempt led to the development of the MALTA[7] [8] and its second generation MALTA2[9][10] pixel detectors aiming for HL-LHC. All the characteristics of the detector are to be studied before its use in an actual detector. One such property is fast-timing, which is the delay or time taken between the collision of a particle with the detector and its detection. In this study, a Micro-X-ray source is designed and used to study the Fast timing properties of MALTA and MALTA2 detectors.

2 MALTA and MALTA2 Pixel detectors

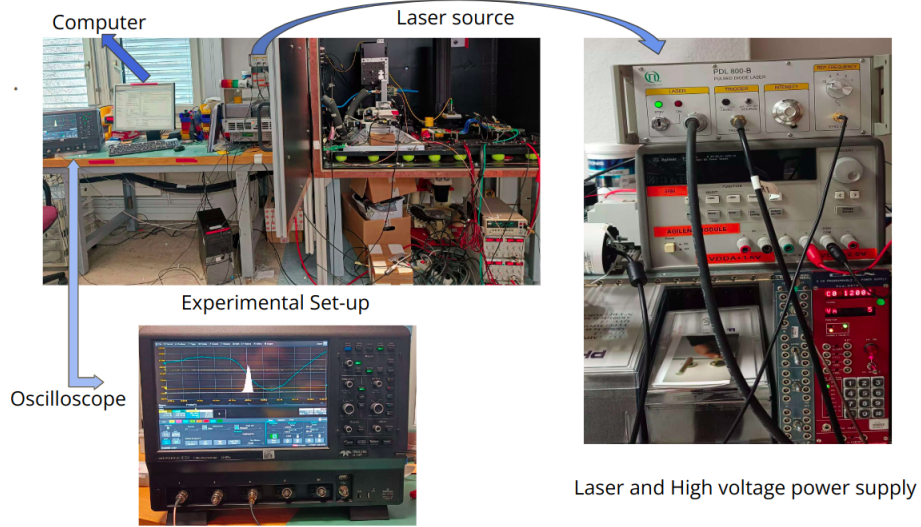
MALTA, designed using Tower-Jazz 180 nm technology[7], is a robust monolithic active pixel detector resilient to radiation exposure up to a fluence in the order of 10^{15} n/cm² and hit rate capability of crossing 100 MHz/cm². With featuring an active area of 18.3 mm² and a 512 × 512 pixel matrix with 36.4 μm² pixels, it boasts a quick pixel response time of up to 20 ns, meeting the HL-LHC's bunch-crossing identification requirements. The chip's asynchronous read-out eliminates the need for clock distribution, reducing power consumption. MALTA features a double-column read-out architecture, and can read out multiple hits per double column. The chip's foundation for read-out lies in the Virtex 7-series FPGA. Connection to a VC707 evaluation board is established through an FMC connector, with a specially designed asynchronous oversampling detecting bits from 40 differential LVDS signals. These bits are then forwarded to a 500 MHz FIFO, subsequently read into the control software via IPBUS[11].

MALTA2,[12] [13]a pixel detector demonstrator, is designed using Tower-Jazz 180 nm Monolithic CMOS technology, measuring 20.2 mm × 10.1168 mm. It is approximately half the size of MALTA, featuring a matrix of 224 × 512 pixels, with each pixel measuring 36.4 μm². Two process modifications(NGAP and extra deep PWELL/XDPW) has been done to increase the in the pixel corners[14]. It is specifically designed to increase the radiation hardness [15] with achieving lower RTs noise in the sensor front-end. There are improvements in MALTA2 slow control by using a shift resistor instead of an Ethernet-like protocol. In the pixel-front end, the implementation of an open loop amplification led to a compact design and low noise and the use of multiple cascode transistors helped in the gain enhancement of the front end[9]. The demonstrator's asynchronous read-out is clock-independent, transmitted through a 37-bit bus, and controlled via a 4322-bit shift register. The read-out includes KC705, a KINTEX7 series of FPGA[16].

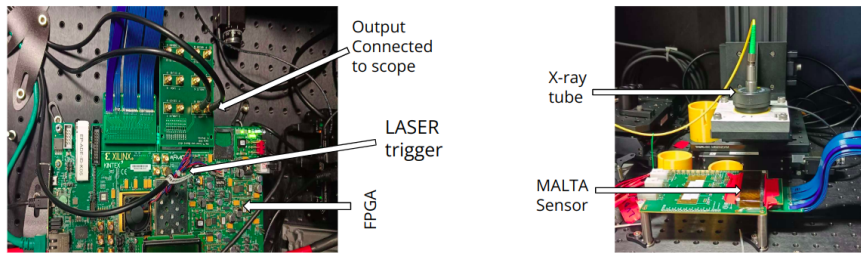
3 Micro-X-ray set-up at CERN

With the bunch-crossing clock of the LHC being 25 ns[17], sensors and read-out architecture have to be sufficiently fast in order to match the hits with the corresponding bunch-crossing. Furthermore, nanosecond level response time resolution is required to contribute to event reconstruction. The fast timing of the chip requires examination prior to their usage in a detector. Traditionally, this investigation involves reflecting a laser beam off the detector and analyzing the discrepancy between the input and output signals[18]. However, this laser technique proves inadequate for the MALTA2 due to significant reflection issues with the detector's front-end electronics[7], which interfere with accurate timing measurements.

To circumvent these challenges, we have opted for X-rays because of their ability to penetrate the metal layers of the detector without reflection. This does not require a high-end X-ray machine. Instead, we have developed a micro X-ray system, as shown in Figure 1, capable of emitting X-rays in response to laser exposure. This approach employs a micro X-ray source that generates short pulses from Cu-Cr targets specifically designed for this application. For the purpose of characterizing the timing performance of the MALTA2, our triggered X-ray set-up plays an important role. Initially, the timing response of the X-ray itself is measured using the LGAD [19]. This baseline measurement



(a)



Triggering FPGA and readout

X-Ray tube with linear stage for focusing X-rays

(b)

Figure 1: Figure illustrates the devices used for the study and the connections between them. In (a), The upper left plot shows the complete set-up with the representation of a laser, a High voltage source for X-ray generation, and an oscilloscope. In the left plot in (b), the Kintex7 KC705 FPGA is shown, which is used to trigger the laser and also helps us in signal processing. The right figure in (b) shows the MALTA sensor with the designed micro X-ray tube, held by a linear stage 10 cm above the chip.

serves as a reference for further comparison with the MALTA2's timing response, enabling us to achieve a comprehensive understanding of the detector's timing capabilities.

3.1 Micro-X-ray source

X-rays are generated by utilizing a 16 mm elongated tube featuring a photo-cathode and anode composed of chromium and copper fabricated above a Beryllium window. Electrons are liberated from the photo-cathode via the photoelectric effect initiated by a laser beam. Subsequently, these emitted electrons undergo acceleration through the application of a 12kV electric field within the

tube. The interaction of these accelerated electrons with the target material in the anode produces X-rays, including bremsstrahlung and fluorescence. The X-ray production process is illustrated in Figure 2. The emitted X-rays exhibit a random trajectory in space. With the increased applied voltage to the X-ray tube, the number of generated photons increases due to the formation of new transition lines.

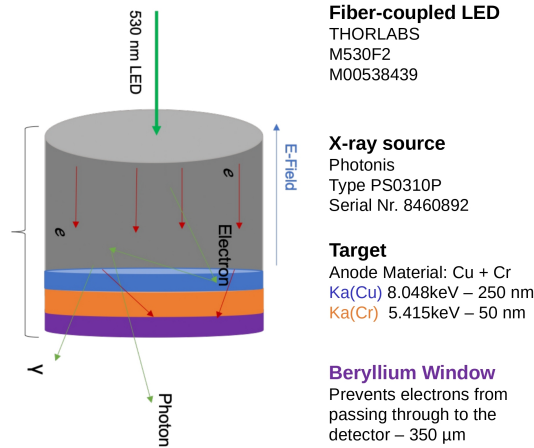


Figure 2: Illustrative description of Micro X-ray source. It is connected to a 530 nm laser source that falls on the cathode. The anode material is made with 250 nm copper and 50 nm chromium, which generates x-rays after interacting with accelerated electrons. Finally, there is a beryllium window that prevents electrons from passing through it.

3.2 Geant4 Simulation for X-ray tube

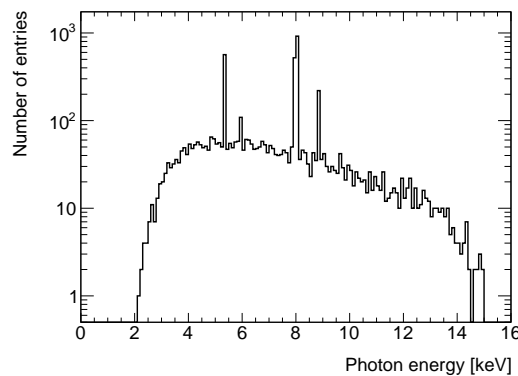


Figure 3: Geant4 Simulation of the photon energy generated from the Micro X-ray tube. The x-axis shows the energy of the generated photons in the keV scale. Four peaks are visible, with two more prominent peaks at 5.41 and 8.04 keV corresponding to k_{α} energy peaks of Cr and Cu.

A Geant 4 simulation was conducted to analyze the energy variation of emitted photons from a X-ray tube. The simulation results in Figure 3 show distinct peaks at 5.4 and 8 keV, corresponding to

the characteristic lines (k_α) of copper and chromium along with two distinct k_β lines. Subsequently, experimental validation of these findings was undertaken using an LGAD (Low Gain Avalanche Detector) because of its high granularity and precise timing capabilities.

4 Test set-up with LGAD

LGAD, the Low-Gain Avalanche Detector[19][20] is a type of silicon detector used in particle physics experiments. The utilization of LGAD in this experimental phase is particularly advantageous, as it enables us to achieve optimal timing resolutions[21], a crucial factor in accurately characterizing X-ray emission. The LGAD experimental arrangement is illustrated in the accompanying schematic diagram, as shown in Figure 4. In this set-up, laser beams are generated and guided onto a micro X-ray source, initiating the generation of X-rays. The resultant X-rays are directed toward the LGAD, and the corresponding signals are captured and recorded using an oscilloscope. Simultaneously, we have directly utilized the LGAD signal to access the energy of the emitted photons based on the amplitude of the LGAD signal. This approach provides a direct and efficient mean of evaluating the photon energy within our experimental framework.

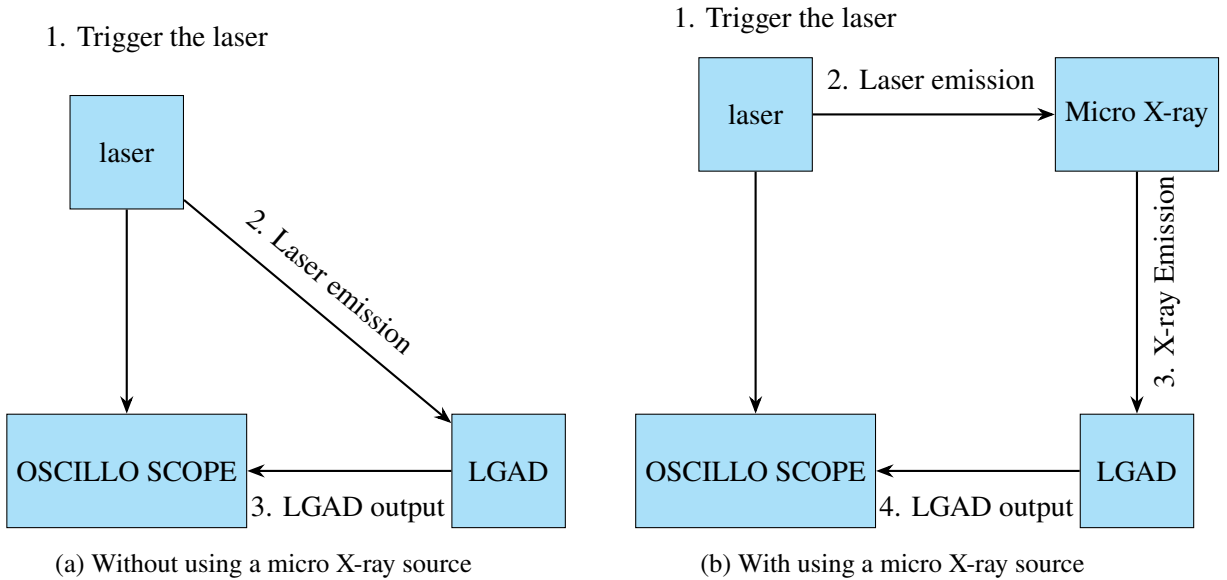


Figure 4: LGAD set-up illustrating the working flow of the set-up. In (a), we are focusing the laser directly on LGAD, and in (b), an additional Micro-Xray source is used. The laser emission and detection time information are collected and compared in both cases using the oscilloscope.

5 Results from LGAD

We conducted two key studies utilizing the Low Gain Avalanche Diode. The first study focused on characterizing the energy peaks generated by the X-ray source. This aspect is necessary to understand the X-ray tube's performance and ensure its suitability for our applications. The second study delved into analyzing the timing precision of the X-ray source by examining the standard

deviation of its delay. For the same, we compared the performance of the micro X-ray source, activated by laser exposure, against a standalone laser source. These preliminary analyses are important in evaluating the contribution of the X-ray set-up toward total delay to ensure precise timing measurements in our experimental framework.

5.1 Characterization of Micro X-ray tube

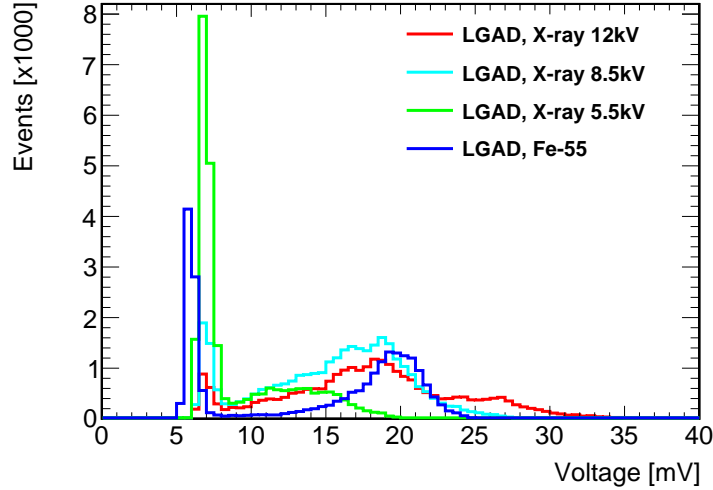


Figure 5: Comparison of the signal amplitudes using LGAD with Fe^{-55} and X-ray sources as a function of voltage measured from the LGAD. The two peaks are visible for the signal using X-rays generated at 12kV supply voltage, corresponding to Cr and Cu K_{α} lines. The peaks of the red line representing the amplitude of the signal using an X-ray tube at 12kV are compared with the peak from the Fe^{-55} -source(blue)

In this study, we quantify the energy of photons using the LGAD signal, represented on the X-axis in terms of voltage and exhibit a linear relationship with energy. We employed a Fe^{-55} source with known energy associated with alpha decay to establish a calibration framework. The measured energy from the alpha decay was subsequently compared with the energies of X-rays generated at voltages of 5.5 kV, 8.5 kV, and 12 kV. Notably, the X-rays produced under a 12 kV voltage setting revealed distinct peaks at 5.4 kV and 8 kV, explaining the nuanced energy characteristics inherent in the X-ray emission process. With the increasing energy of the X-ray photon, the energy of the electron emitted increases, increasing the signal voltage. A comparison of peaks is shown in Figure 5. The peak is parametrized using Gaussian and polynomial functions, as shown in Figure 6. The results from the fit are summarized in Table 1, which matches the theoretical value of k_{α} lines from chromium and copper.

5.2 Timing performance of LGAD

In this investigation, the LGAD was characterized by utilizing a laser beam, yielding a timing resolutions below 50ps, where the resolution has contributions from both LGAD and the laser

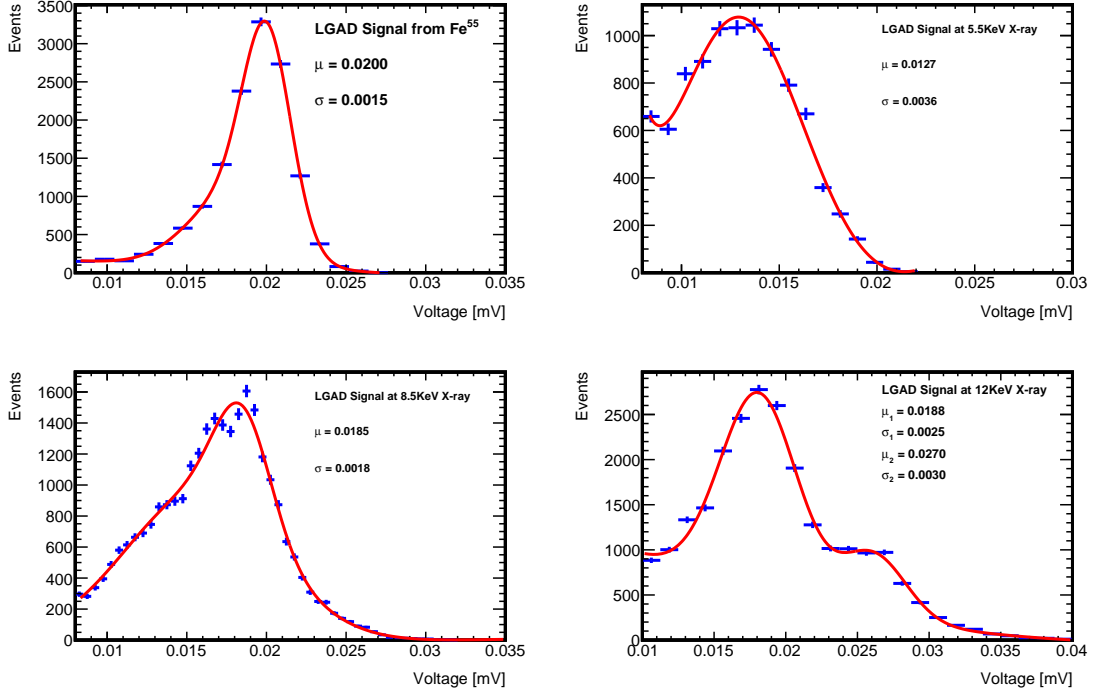


Figure 6: The subplots show a comparison between the fitting parameters of generated signal amplitude using LGAD with Fe and X-ray sources at 5.5 keV, 8.5 keV, and 12 keV. The x-axis represents the energy of generated electrons from LGAD using the sources, while the y-axis represents the number of events. The two peaks are visible for the signal amplitude using X-rays generated at 12 kV supply voltage.

Table 1: Summary of the fit results

Peak	Value	Energy (Theoretical value)	Energy (Observed value)
Fe source	0.02	5.9 keV	5.9 keV
Peak from 8.5 keV Cr	0.0185	5.41 keV	5.45 keV
Peak from 8.5 keV Cr	0.0188	5.41 keV	5.54 keV
Peak from 8.5 keV Cr	0.0270	8.04 keV	7.96 keV

source. Subsequently, the entire system was engaged to generate X-rays through laser irradiation. Through analysis of the X-ray signals, the timing resolution is determined to be approximately 300ps across varying laser frequencies, which can be seen in Figure 7. This evaluation allowed us to draw a conclusive inference: the timing resolution of the Micro-X-ray source is estimated to be in the proximity of 250ps, demonstrating its efficiency and reliability in temporal measurements. These findings underscore the potential of our system for applications demanding precise timing resolution in the realm of X-ray generation and detection.

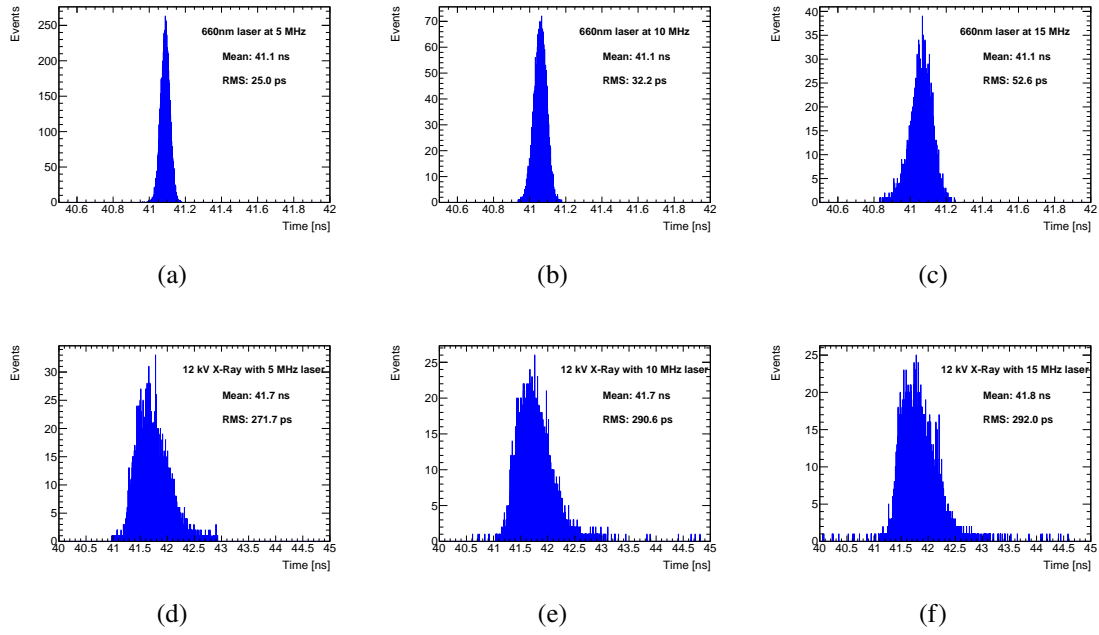


Figure 7: Comparison of the timing delay between the laser trigger and LGAD signal detection time using laser and X-rays. The laser frequency is varied from 5 to 15 MHz, and the RMS of the delay are compared with and without using a micro-X ray source. The RMS of the timing delay using the micro-XRay tube with laser is found to be approximately 250 ps higher than the RMS of timing delay without using the micro-XRay tube, concluding the contribution of approximately 250 ps from the micro-XRay tube towards the RMS of the delay.

6 Measurements with MALTA and MALTA2

6.1 Measurements using MALTA sample

In contrast to the LGAD set-up, the MALTA system employs an internal trigger from the FPGA to initiate the laser, which is subsequently directed toward the X-ray tube for X-ray emission as described in Figure 8. The operational sequence involves triggering the FPGA using software, whereby the KINTEX-7 FPGA activates the laser source. As the laser beam interacts with the X-ray tube, X-rays are emitted and directed toward the MALTA sensor (W11R12, which is a 100 nm thick sensor with a p-type Czochralski substrate with an extra deep p-well implant). The timing information is gathered within the FPGA and transmitted to the oscilloscope. The oscilloscope then performs a comparison of the timing data, enabling the determination of delay information. This delay information is necessary for analyzing the temporal characteristics of MALTA where we can subtract the effect of previously measured micro X-ray source, which is approximately 300 ps. Notably, the timing performance of MALTA is observed to operate on a nanosecond scale, showcasing its capability for precise measurements.

6.2 Measurements using MALTA2 sample

While the set-up for the MALTA2 chip mirrors that of MALTA, distinctions in the MALTA2 configuration necessitate corresponding alterations in connection and firmware. Specifically, the

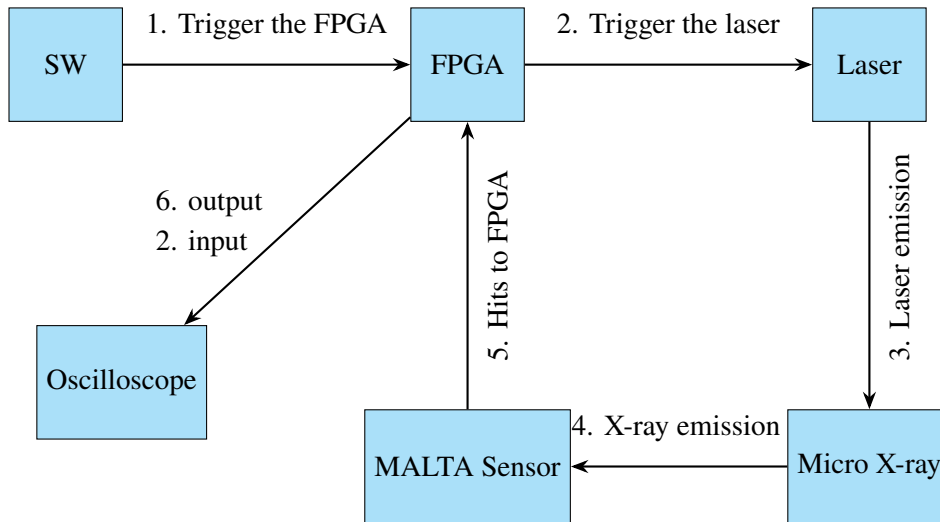


Figure 8: This represents the Schematic diagram for the MALTA testing layout illustrating the working flow of the experimental set-up. Upon instructions, FPGA triggers the laser and sends the actual triggering time to our oscilloscope. The laser falls on the X-ray tube, resulting in X-ray emission. The sensor detects the X-ray exposure and sends the detection time to the oscilloscope

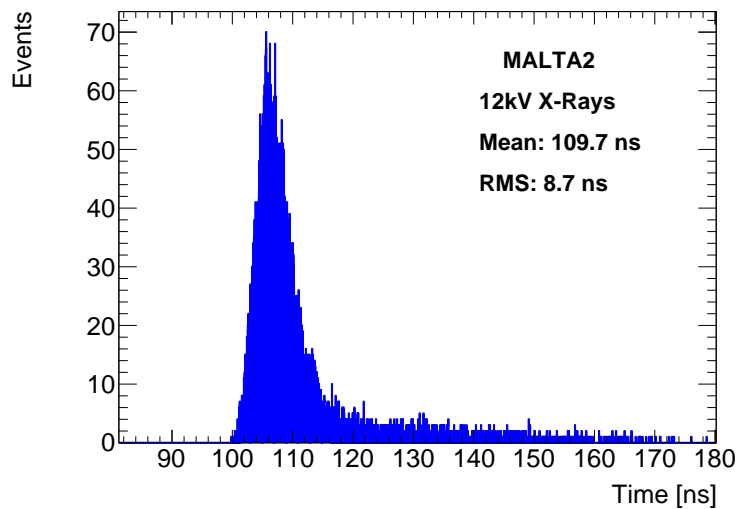


Figure 9: Delay between the input and output signals using 12kV X-rays on the MALTA2 sample. The contribution to the tail part comes from the corner pixel hits, front-end electronics as well as due to comparison errors from the oscilloscope.

default FPGA firmware for MALTA2 is changed accordingly to receive signals from the computer, subsequently triggering the laser and capturing the timing information when X-rays interact with the laser. These firmware modifications are crucial to facilitate the transmission of signals to the oscilloscope, ensuring data collection and analysis. The timing study of the MALTA2, Epitaxial

chip with an extra deep p-well implant is done over a several range of high voltages with different threshold values. The delay for 12kV voltage can be seen in Figure 9 below.

7 Results

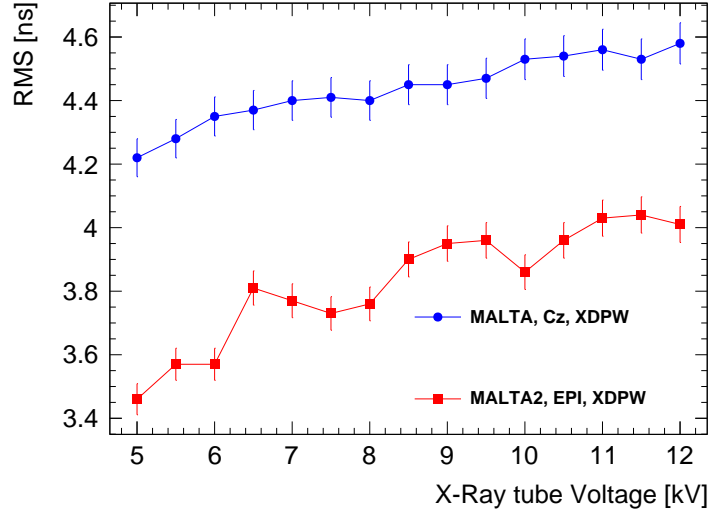


Figure 10: Comparison between RMS of the timing delay of MALTA and MALTA2 samples using the first 25 ns only. The x-axis shows the input voltage provided to the micro X-ray tube, and the y-axis is the standard deviation of the delay in the first 25 seconds. The timing delay contributions from the set-up are included for both the MALTA and MALTA2 samples.

A distinct and extended tail is evident in both the MALTA and MALTA2 datasets, and it is crucial to emphasize that this phenomenon is not solely attributed to timing differences. Rather, the presence of such pronounced tails can be largely attributed to errors introduced by the oscilloscope. A contribution to the tail part also comes from MALTA front-end electronics. The underlying mechanism involves the acquisition of two distinct signals from the FPGA in the oscilloscope—one originating from the trigger and the other from the MALTA2 output. Notably, these signals are characterized by the presence of multiple peaks rather than a singular peak. Our approach to determining the timing difference involves the selection of corresponding peaks; however, occasional discrepancies result in the acceptance of the timing associated with the subsequent peak rather than the intended one, leading to the augmentation of data points in the far-tail region. In response to this effect, we adopted two distinct methodologies. Initially, we sought to ascertain the root mean square (RMS) value by excluding the prolonged tail and focusing solely on the initial 25 ns (bunch crossing time for LHC), as shown in Figure 10. From this plot, it is evident that the RMS is increasing with the applied voltages to the X-ray tube, which is solely due to the involvement of a higher number of transition lines in Cu and Cr at higher applied voltage.

Subsequently, an alternative approach involved a comparative analysis of the peak width for both MALTA2 and MALTA datasets. Despite the fact that these peaks do not match perfectly to

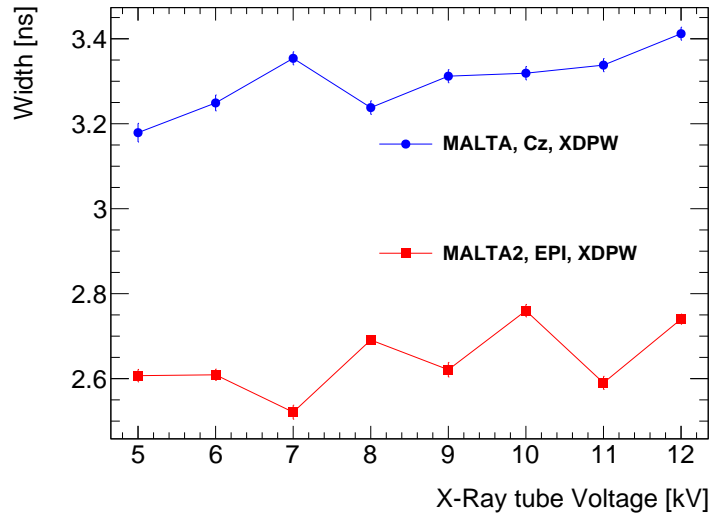


Figure 11: Comparison between the standard deviation of the timing delay of MALTA and MALTA 2 samples using the Gaussian fit method. The peaks are fitted with a single Gaussian, and the width of the Gaussian fit is compared for MALTA and MALTA2 at different X-ray tube voltages. The x-axis shows the input voltage provided to the micro X-ray tube, and the y-axis is the standard deviation of the Gaussian fit. The timing delay contributions from the experimental set-up are included for both the MALTA and MALTA2 samples.

Gaussian fits, for the sake of general applicability, our analysis considered only single Gaussian fits to derive approximate values. Then, we compared the width values of MALTA and MALTA2 from the fit at different applied voltages to the X-ray tube.

From Figure 11, we found the RMS of the peak is approximately 2.6 ns for MALTA2 with a best value of 2.5 ns, where it has contributions from the set-up (approximately 300 ps), jitter from FPGA (approximately 160 ps) and jitter from the laser source (up to 50 ps) that affects the final value. After correcting these values, the RMS value of the fast timing was found to have the best value of 2 ns -2.1 ns for the MALTA2 epitaxial sample. Similarly, For MALTA, we find the RMS of the peak is approximately 3.3 ns with a best value of 3.2 ns. After the corrections from the system, we find the fast timing resolution within a best value of 2.7 ns to 2.8 ns. In this case, we can see consistent values, unlike in Figure 10, as we have less contribution of photons generated from higher transition levels towards the peak values. Also, as the resolution of the MALTA sensor is predicted to be 100 ps, we can clearly see that the values of RMS at different X-ray tube voltages are compatible within 2σ . It gives us a strong sign regarding the consistent width of the Gaussian fit of the peak values. In both cases, we have found significantly better timing precision for the MALTA2 than the MALTA sensor. From the test beam data collected between 2021-2023, The best value of the timing resolution achieved for MALTA2 with czochralski substrate at a low threshold settings is 1.7 ns using a cluster size of 2 pixels [13]. As the (σ) of the malta sensor is 100 ps, our findings with the MALTA2 epitaxial substrate match with the test beam data with a 3σ standard deviation.

8 Conclusion

The study was focused on investigating the deviation in the delay time of MALTA and MALTA2 epitaxial samples. Given the limitations of conventional laser techniques, we employed a micro X-ray source comprising copper and chromium layers to generate X-rays. The utilization of a Low-Gain Avalanche Detector (LGAD) allowed for a comprehensive exploration of the properties of the Micro-X-ray source, and we observed that the k_α energy levels were consistent with theoretical values. The findings revealed that the micro X-ray source contributed approximately 300 ps to the overall delay time for different laser frequencies, as determined through laser source experiments. Also, the FPGA is found to have a contribution of approximately 80 ps, resulting in the RMS of the delay from MALTA and MALTA2 EPI samples to be approximately 2.8 ns and 2.1 ns with a best value of 2.7 ns and 2 ns, respectively. Also, this experiment concluded the delay time improvement for the second generation of MALTA pixel detectors than its previous generation, providing strong support for its usability in future collider experiments.

Acknowledgments

This project has received funding from the European Unions Horizon 2020 Research and Innovation programme under Grant Agreement numbers: 101004761 (AIDAinnova), 675587 (STREAM), 654168 (AIDA-2020). Also, we thank Science and Engineering Research Board, India and the Ministry of Human Resource Development, India for their funding support.

References

- [1] G. Garcia-Sciveres et al., *A review of advances in pixel detectors for experiments with high rate and radiation*, *Rept. Prog. Phys.* **81** (2018) 066101.
- [2] G. Apollinari et al., *High-Luminosity Large Hadron Collider (HL-LHC)*, Technical Design Report V. 0.1, [CERN-2017-007-M](#).
- [3] The ATLAS collaboration, *Technical Design Report for the ATLAS Inner Tracker Pixel Detector*, [CERN-LHCC-2017-021](#) (2017).
- [4] H. Pernegger et al., *First tests of a novel radiation hard cmos sensor process for depleted monolithic active pixel sensors*, *JINST* **12** (2017) P06008.
- [5] G. A. Rinella and ALICE collaboration, *The ALPIDE pixel sensor chip for the upgrade of the ALICE Inner Tracking System*, *Nucl. Instrum. Meth. A* **845** (2017) 583.
- [6] I. Berdalovic et al., *Monolithic pixel development in TowerJazz 180 nm CMOS for the outer pixel layers in the ATLAS experiment*, *JINST* **13** (2018) C01023.
- [7] H. Pernegger et al., *Monolithic pixel development in TowerJazz 180 nm CMOS for the outer pixel layers in the ATLAS experiment*, *Nucl. Instrum. Meth. A* **924** (2019) 92.
- [8] R. Cardella et al., *MALTA: an asynchronous read-out CMOS monolithic pixel detector for the ATLAS High-Luminosity upgrade*, *JINST* **14** (2019) C06019.
- [9] F. Piro et al., *A 1- μ W radiation-hard front-end in a 0.18- μ m CMOS process for the MALTA2 monolithic sensor*, *IEEE Trans. Nucl. Sci.* **69** (2022) 1299.

- [10] M. van Rijnbach et al., *Radiation hardness and timing performance in MALTA monolithic pixel sensors in TowerJazz 180 nm*, *JINST* **17** (2022) C04034.
- [11] L. Flores Sanz de Acedo et al., *Design of large scale sensors in 180 nm CMOS process modified for radiation tolerance*, *Nucl. Instrum. Meth. A* **980** (2020) 164403.
- [12] D. V. Berlea et al., *Radiation hardness of MALTA2, a monolithic active pixel sensor for tracking applications*, *IEEE Trans. Nucl. Sci.* **70** (2023) 2323.
- [13] M. van Rijnbach et al., *Radiation hardness of MALTA2 monolithic CMOS imaging sensors on Czochralski substrates*, *Eur. Phys. J. C* **84** (2024) 251.
- [14] M. Munker et al., *Simulations of CMOS pixel sensors with a small collection electrode, improved for a faster charge collection and increased radiation tolerance*, *JINST* **14** (2019) C05013.
- [15] M. Dyndal et al., *Mini-MALTA: radiation hard pixel designs for small-electrode monolithic CMOS sensors for the High Luminosity LHC*, *JINST* **15** (2020) P02005.
- [16] L. Flores Sanz de Acedo et al., *Latest developments and characterisation results of DMAPS in TowerJazz 180nm for High Luminosity LHC*, *J. Phys. Conf. Ser.* **2374** (2022) 012074.
- [17] O. Brüning and L. Rossi, *The High Luminosity Large Hadron Collider–HL-LHC*, *The High Luminosity Large Hadron Collider: New Machine for Illuminating the Mysteries of the Universe* (2024) 1.
- [18] D. Hohov et al., *Developing an accurate and robust tool for pixel module characterization*, *JINST* **17** (2022) P03009.
- [19] G. Pellegrini et al., *Technology developments and first measurements of Low Gain Avalanche Detectors (LGAD) for high energy physics applications*, *Nucl. Instrum. Meth. A* **765** (2014) 12.
- [20] M. Carulla et al., *50 μm thin Low Gain Avalanche Detectors (LGAD) for timing applications*, *Nucl. Instrum. Meth. A* **924** (2019) 373.
- [21] L. Diehl et al., *Comparison of the time resolution of unirradiated and irradiated LGADs and 3D sensors*, *Nucl. Instrum. Meth. A* **1046** (2023) 167691.